


Photoacids Hot Paper
How to cite: *Angew. Chem. Int. Ed.* **2022**, *61*, e202200709

International Edition: doi.org/10.1002/anie.202200709

German Edition: doi.org/10.1002/ange.202200709

Electronic Structure Changes of an Aromatic Amine Photoacid along the Förster Cycle

Sebastian Eckert,* Marc-Oliver Winghart, Carlo Kleine, Ambar Banerjee, Maria Ekimova, Jan Ludwig, Jessica Harich, Mattis Fondell, Rolf Mitzner, Ehud Pines,* Nils Huse, Philippe Wernet,* Michael Odelius,* and Erik T. J. Nibbering*

Abstract: Photoacids show a strong increase in acidity in the first electronic excited state, enabling real-time studies of proton transfer in acid-base reactions, proton transport in energy storage devices and biomolecular sensor protein systems. Several explanations have been proposed for what determines photoacidity, ranging from variations in solvation free energy to changes in electronic structure occurring along the four stages of the Förster cycle. Here we use picosecond nitrogen K-edge spectroscopy to monitor the electronic structure changes of the proton donating group in a protonated aromatic amine photoacid in solution upon photoexcitation and subsequent proton transfer dynamics. Probing core-to-valence transitions locally at the amine functional group and with orbital specificity, we clearly reveal pronounced electronic structure, dipole moment and energetic changes on the conjugate photobase side. This result paves the way for a detailed electronic structural characterization of the photoacidity phenomenon.

Introduction

It is well established that electronic excitation of photoacids induces enhanced acidity with concomitant changes in hydrogen bond interactions, changes in acid-base equilibria and increase in proton dissociation rates. This feature has been extensively utilized with much success in studies of proton transfer and proton transport dynamics in solution at ultrafast time scales, ranging from acid-base neutralization reactions in water^[1] to proton transfer in protic and aprotic solvents,^[2] as well as in media used in hydrogen fuel cells.^[3] Photoacids are also recognized as essential chromophores in the function of biosensor proteins like green fluorescent protein.^[4] Photoacids are typically organic aromatic systems with a proton releasing group (aromatic alcohols R–OH, or protonated aromatic amines, cationic acids, R–NH₃⁺). A wide range of photoacid molecules were developed as molecular probes (as tools to derive local pK_a-values and local pH conditions). Theodor Förster is the first who has explained the photo-physics of photoacids, using a thermodynamic cycle, what is now denoted as the Förster cycle (see Figure 1a), connecting electronic transition frequencies of the photoacid (R–OH or R–NH₃⁺) and its conjugate photobase (R–O[−] or R–NH₂) with electronic ground-state and excited state acidities (with pK_a- and pK_a^{*}-values, respectively).^[5] The underlying mechanisms for promoting photoacidity and photobasicity have, however, remained

[*] Dr. S. Eckert, Dr. M.-O. Winghart, C. Kleine, Dr. M. Ekimova, J. Ludwig, Dr. E. T. J. Nibbering
Max Born Institut für Nichtlineare Optik und Kurzzeitspektroskopie
Max Born Strasse 2A, 12489 Berlin (Germany)
E-mail: sebastian.eckert@helmholtz-berlin.de
nibberin@mbi-berlin.de

Dr. A. Banerjee, Prof. Dr. M. Odelius
Department of Physics, Stockholm University, AlbaNova University Center
106 91 Stockholm (Sweden)
E-mail: odelius@fysik.su.se

J. Harich, Prof. Dr. N. Huse
Institute for Nanostructure and Solid State Physics, Center for Free-Electron Laser Science
Luruper Chaussee 149, 22761 Hamburg (Germany)

Dr. M. Fondell, Dr. R. Mitzner
Institute for Methods and Instrumentation for Synchrotron Radiation Research, Helmholtz-Zentrum Berlin für Materialien und Energie GmbH
Albert-Einstein-Strasse 15, 12489 Berlin (Germany)

Prof. Dr. E. Pines
Department of Chemistry, Ben Gurion University of the Negev
P.O.B. 653, Beersheva 84105 (Israel)
E-mail: epines@bgu.ac.il

Prof. Dr. P. Wernet
Department of Physics and Astronomy, Uppsala University
Box 516 Lagerhyddsvägen 1, 751 20 Uppsala (Sweden)
E-mail: philippe.wernet@physics.uu.se

© 2022 The Authors. Angewandte Chemie International Edition published by Wiley-VCH GmbH. This is an open access article under the terms of the Creative Commons Attribution Non-Commercial NoDerivs License, which permits use and distribution in any medium, provided the original work is properly cited, the use is non-commercial and no modifications or adaptations are made.

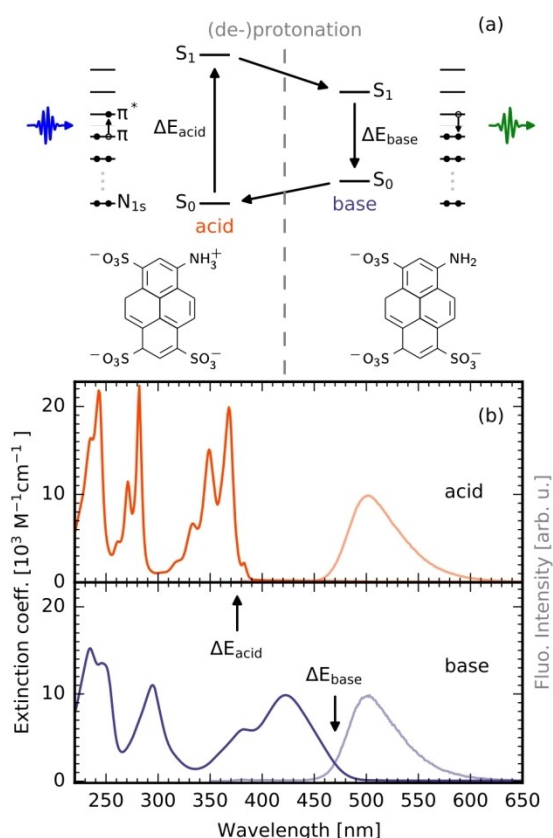


Figure 1. a) Förster cycle of APTS, showing the electronic states involved. As the $pK_a^* < 0$ the S_1 energy level of APTS in its base form is lower than in its acid form, while for weaker photoacids with $pK_a^* > 0$ the opposite occurs. Molecular structures of APTS in its acid and base forms are shown underneath; b) Electronic absorption and fluorescence spectra of APTS in its acid and base forms. Fluorescence emission of APTS, initially excited in its acid form, is almost exclusively due to APTS in its base form, as proton transfer occurs on a much shorter time scale than the electronic excited state decay.

elusive and one of the reasons for that has been the challenge to reveal the coupled dynamics of intramolecular electronic structure changes and intermolecular hydrogen bonding interactions. Classical pictures suggest that the electronic excitation causes a change in charge density in the proton donating moiety of the photoacid increasing its acidity.^[6] Other studies have suggested rather a major effect due to more extensive electronic charge distributions in the electronic excited state of the conjugate base side of the Förster cycle.^[7] A rationalization in terms of electronic state-dependent differences in conjugation of the proton donating group with the aromatic ring system in terms of aromaticity and anti-aromaticity^[8] has also been reported.^[9] From experiments a determination of electronic structure changes of photoacids has only been partial, through electronic excitation induced solvent shell rearrangements as probed with UV/Vis pump-probe spectroscopy,^[11-k] or by local probing of hydrogen bond strengths as demonstrated with UV/IR spectroscopic measurements of photoacid-base complexes.^[10]

Pyrene photoacids have been widely used in ultrafast proton transfer and solvation dynamics studies.^[11] While the pyrene aromatic ring system forms the backbone, the proton donating functionality is usually provided by a hydroxyl or protonated amine group, and substituents at the 1,3 and 6-positions may enhance solubilities in polar solvents, with the caveat of possible changes in $^1L_a/^1L_b$ excited state energies and/or electronic state mixing.

Here we report on a new approach where we locally probe the electronic structure changes of the proton donating amine-group of 8-aminopyrene-1,3,6-trisulfonate (APTS, see Figure 1a) in aqueous solution, by use of picosecond nitrogen K-edge absorption spectroscopy. Its potential to locally probe electronic structure upon photo-induced proton transfer tautomerization has been demonstrated in previous studies.^[11] Upon electronic $S_0 \rightarrow S_1$ excitation, we follow the response of the nitrogen core-to-valence transitions from the nitrogen 1s to the lowest unoccupied molecular orbitals (N 1s \rightarrow LUMOs) of APTS in its photoacid and its conjugate photobase forms, thereby fully mapping out the electronic structural dynamics along the four stages of the Förster cycle, from the perspective of the proton donating moiety of the photoacid.

The protonated amine-based cationic pyrene photoacid APTS $R-NH_3^+$ shows an $S_0 \rightarrow S_1$ electronic absorption band between 320–380 nm much akin to that of aromatic pyrene (Figure 1b). The conjugate photobase $R-NH_2$ has its $S_0 \rightarrow S_1$ electronic absorption located between 350–470 nm. The emission properties of APTS in either its photoacid $R-NH_3^+$ or its conjugate photobase $R-NH_2$ spectrally strongly overlap, as APTS changes its acidity from $pK_a(S_0) = 2.3$ to at least $pK_a^*(S_1) = -7$ in aqueous solution and a net proton transfer of the photoacid occurs to create its conjugate photobase.^[12] Upon electronic excitation, proton transfer to the solvent water occurs with a 30 ps time constant in H_2O , with a remarkably large kinetic isotope effect (KIE) of about 5, i.e. in D_2O the dissociation time increases to 150 ps.^[13] Only in strong mineral acid solvents a significant contribution of fluorescence comes from its APTS photoacid form.^[12] To better match the 90 ps temporal resolution of the UV-soft X-ray pump-probe set-up at BESSYII with our benchmarking study here, we decided to study APTS in deuterated water, where the photoinduced APTS photoacid \rightarrow APTS conjugate photobase conversion is governed by slower deuteron transfer dynamics that can be better probed with the time resolution of our experiment.

Results and Discussion

Steady-state nitrogen K-edge absorption spectra of APTS in its photoacid $R-ND_3^+$ and its conjugate photobase $R-ND_2$ are shown in Figure 2. Here we have recorded X-ray absorption spectra (XAS) in transmission mode using flatjet technology^[14] at the UE52_SGM beamline at BESSYII.^[15] We compare the experimental spectra with those obtained with (time-dependent) density functional theory ((TD)-DFT/CAM-B3LYP)^[16] calculations for ground state XAS. To compare XAS features in the electronic ground and

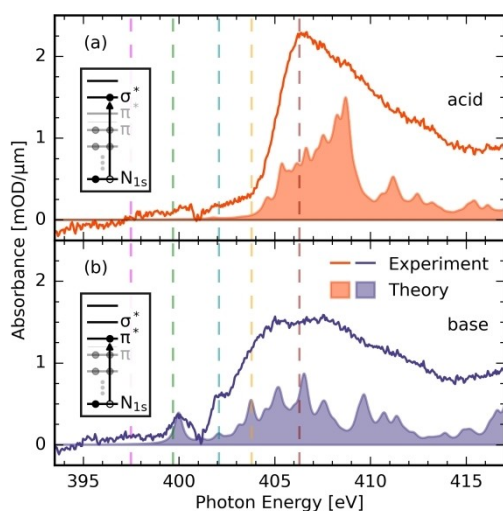


Figure 2. Nitrogen K-edge absorption spectra of electronic ground state APTS in its R-ND_3^+ acid and R-ND_2 base forms (solid lines) at a concentration of 50 mM. Dashed lines at 397.5 eV, 399.7 eV, 402.1 eV, 403.8 eV, and 406.3 eV are relevant for the comparison with transient absorption spectral features as displayed in Figure 3. Calculated spectra spanning the whole energy window, obtained with TDDFT CAM-B3LYP/def2-SVP/CPCM level of theory (see Supporting Information), indicate that the first strong transitions for the acid are of $1s \rightarrow \sigma^*$ character, whereas for the base form we also observe distinct pre-edge $1s \rightarrow \pi^*$ transitions.

excited states, we also performed complete active space self-consistent field/ n -electron valence perturbation theory CASSCF/NEVPT2 calculations^[17] for ground and excited state XAS (using the ORCA quantum chemistry package^[18]), on the solute with a limited number of water solvent molecules (see Supporting Information for further details on experiments and calculations, including additional comparison of measured and calculated UV/Vis spectra, and the chosen active orbitals).

APTS in its photoacid R-ND_3^+ form has a single broad absorption band without substructure, with a maximum absorbance at 406.3 eV, and a width of about 5 eV, with an asymmetry resulting from a steeper rising edge than the falling edge. Instead its conjugate photobase R-ND_2 shows an N K-edge spectrum richer in structure, with narrow resonances at 400 and 402 eV, and a 7 eV broad absorption band centred at 406.5 eV. This result immediately shows that the protonation state of APTS strongly affects the nitrogen K-edge XAS probing excitations from the amine nitrogen $1s$ core to unoccupied molecular orbitals of APTS.

Our calculated XAS in Figure 2 reveals the underlying reasons for these marked differences observed for APTS in acid and base forms. For APTS in its electronic ground state photoacid form the nitrogen K-edge spectrum is governed by $1s$ core excitations to N–H and N–C σ^* orbitals of the protonated amine group. These transitions are grouped in a relatively narrow spectral range, resulting in a single band without substructure. This is much akin to previously reported nitrogen K-edge spectra of ethylammonium ions $(\text{C}_2\text{H}_5)_y\text{NH}_{4-y}^+$ ($y=0\dots4$) in aqueous solution.^[19] With its positive charge of the protonated amine group and the

pyramidal sp^3 hybridization of the amine nitrogen atom, the nitrogen K-edge XAS is dominated by main-edge N–H and N–C $1s \rightarrow \sigma^*$ transitions around 406.3 eV. Post-edge N–H $1s \rightarrow \sigma^*$ transitions above 406.3 eV are affected by hydrogen bonding interactions with the solvent and pre-edge transitions that, if present, would show up as shoulders or extra peaks well below the main absorption edge, have small absorption cross sections.^[19] For APTS in its electronic ground state photobase form on the other hand the number of transitions contributing to the nitrogen K-edge XAS is larger than is the case for ammonia and the alkylamines. The nitrogen $1s \rightarrow \text{N–H } \sigma^*$ transitions occur for the neutral amine group at ≈ 3 eV lower transition energies, because the amine group is not charged and we have post-edge nitrogen $1s \rightarrow \text{N–H}$ and N–C σ^* contributions in a similar fashion as for ammonia and alkylamines $(\text{C}_2\text{H}_5)_x\text{NH}_{3-x}$ ($x=0\dots3$).^[19] Importantly, the hybridization of the nitrogen lone pair on the non-protonated amine group with the pyrene aromatic C p -orbitals enables in addition a large cross section for a number of nitrogen $1s \rightarrow \pi^*$ LUMO transitions, that are located at significantly lower transition energies, resulting in a pre-edge transition to the LUMO of APTS in the electronic ground state at 400.0 eV.

We show in Figure 3 our results obtained for the transient N K-edge XAS signals, recorded at characteristic values of the UV-pump and N K-edge XAS probe pulse delay. Directly upon electronic HOMO \rightarrow LUMO excitation of the photoacid APTS R-ND_3^+ into S_1 electronic absorption manifold at 343 nm (Figure 3a), the electronic charge distribution changes are modest, from the perspective of the proton donating R-NH_3^+ moiety, as is confirmed by our calculations showing that the R-NH_3^+ moiety is not involved in conjugation with the aromatic pyrene ring system. This is evident from the transient spectra (Figure 3b) measured at zero pulse delay, where only small positive absorbance changes occur at 403.8 eV and a bleach signal emerges at 406.3 eV, with even smaller positive absorbance features at 397.4 eV and 399.7 eV. These absorbance changes grow with time and become more evident at larger pulse delay, as the transient spectra show at 60 ps when the deuteron transfer reaction is well underway for a considerable fraction of the photoexcited molecules, or at 600 ps, when most photoexcited molecules have converted from the electronically excited photoacid APTS R-ND_3^+ form (in the S_1 state) to its electronically excited conjugate photobase R-ND_2 (in the S_1 state). These transient absorption and bleach signals then diminish on a nanosecond time scale, almost quantitatively in accordance with $S_1 \rightarrow S_0$ electronic excited state decay (see also Supporting Information). For comparison, we have also recorded the response of the conjugate photobase R-ND_2 upon electronic excitation using a UV pump pulse tuned at 258 nm (Figure 3c). At 40 ps pulse delay, we observe a bleach contribution throughout the steady-state N K-edge absorption spectral range from 402–410 eV. In addition to that transient absorption bands appear at 397.0 eV and 399.0 eV, indicative of $1s$ core excitations that occur in the APTS conjugate photobase R-ND_2 in the S_1 -state. For optical excitation of APTS R-ND_3^+ at 343 nm, the recorded kinetic traces of the bleach

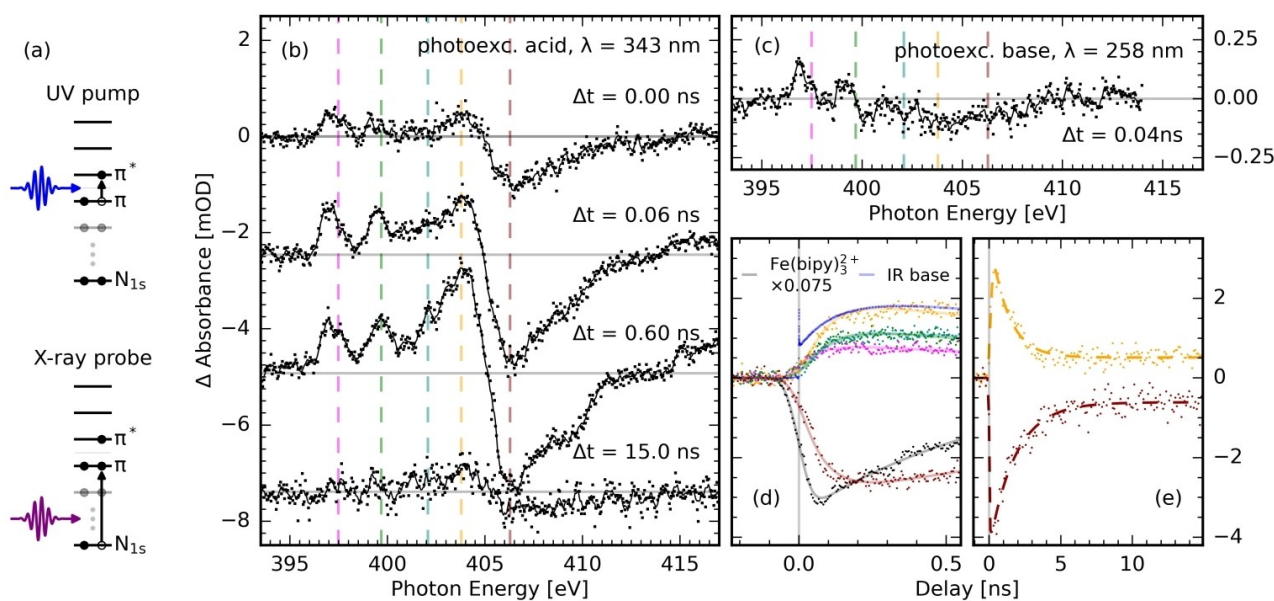


Figure 3. Accessing the Förster cycle of APTS through UV pump–X-ray absorption probe spectroscopy. a) The S_1 state, characterized by a dominant $\pi \rightarrow \pi^*$ transition, is populated by a photo-excitation of the HOMO \rightarrow LUMO ($S_0 \rightarrow S_1$) transition. Consecutive absorbance changes in the nitrogen K-edge spectral range probing the transient population kinetics of the π^* and other electronic states monitor the dynamics of APTS along the Förster cycle. Transient X-ray absorption spectra of the APTS photo-excited in its photoacid (b) and in its photobase (c) forms measured for specific pulse delays, and the time dependence of the transient changes as recorded for APTS photo-excited in its acid form (d), (e) enable us to monitor both the deprotonation process, as well as the transient population of the orbitals involved in the excitation. Dashed lines at 397.5 eV, 399.7 eV, 402.1 eV, 403.8 eV, and 406.3 eV in panels (b), (c) indicate the energies of the kinetic curves with the same colour codes as displayed in panel (d), (e). For comparison we show the build-up dynamics of the excited photobase population obtained from UV/IR pump-probe measurements (see Supporting Information), and have added the transient response of $\text{Fe}(\text{bipy})_3^{2+}$ at 399.5 eV, also photoexcited at 343 nm, that has a bleach signal appearance that is instrument-response limited.^[15b] The slower in-growth of the bleach signal at 406.3 eV for APTS reflects its delayed conversion of APTS $\text{R}-\text{ND}_3^+$ form into APTS $\text{R}-\text{ND}_2$ forms by deuteron transfer in the S_1 -state.

signal at 406.3 eV, and the transient absorption at 397.5 eV, 399.7 eV, and 403.8 eV show a finite increase that can be fitted with a time constant of 80 ps. The temporal onset of this transient signal is clearly delayed with respect to the reference bleach signal upon optical excitation of iron(II)-trisbipyridine $[\text{Fe}(\text{bipy})_3]^{2+}$ defining the zero delay between pump and probe pulses (Figure 3d).^[15b] This shows that the temporal behaviour of the transient absorption bands are correlated with the photoacid APTS S_1 $\text{R}-\text{ND}_3^+ \rightarrow S_1$ $\text{R}-\text{ND}_2$ excited state deuteron transfer reaction. This conclusion has been corroborated with femtosecond UV/IR pump-probe measurements of APTS under identical sample conditions (solute concentration, pD) as those of the picosecond UV/XAS pump-probe experiments (see Supporting Information). The UV/IR pump-probe results measured for different solute concentrations show a concentration-dependent electronic excited state decay. Further support is found in steady-state fluorescence spectra recorded as a function of APTS concentration (see Supporting Information). From this we can conclude that the 1.6 ns decay observed in the UV/XAS pump-probe measurements (Figure 3e) are consistent with a solute concentration-dependent shortening of the APTS S_1 $\text{R}-\text{ND}_2$ excited state lifetime.

APTS has an electronic structure much akin of that of pyrene. For pyrene the first two electronic excited states S_1 and S_2 have been characterized as 1L_a and 1L_b , respectively,

with an optically allowed $S_0 \rightarrow ^1L_a$ (with its transition dipole moment oriented along the long “through axis” direction of the molecule), and a symmetry forbidden $S_0 \rightarrow ^1L_b$ (with its transition dipole moment oriented along the short “through bond” direction of the molecule).^[20] Roos, Reiter and de Vivie-Riedle have reported electronic structure calculations of the S_0 , S_1 and S_2 states of pyrene at the (TD-)DFT/CAMB3LYP/6-31G(d) or CASSCF(4,4)/6-31G(d) levels of theory. They concluded that $S_0 \rightarrow ^1L_b$ is described by two almost equally weighted transitions, from π_2 to π_1^* and from π_1 to π_2^* , respectively. The description of $S_0 \rightarrow ^1L_a$ is dominated by the HOMO \rightarrow LUMO transition, π_1 to π_1^* , and the transition π_2 to π_2^* is less important.^[21]

For pyrene derivatives with electron withdrawing or donating groups at particular positions of the hydrocarbon aromatic molecular system, one may anticipate a different level of electronic excited state mixing compared to that of pyrene. For the photoacid APTS $\text{R}-\text{NH}_3^+$ the nature of the electronic excited states and the optical transitions are nevertheless much alike that of pyrene, i.e. the optically strongly active $S_0 \rightarrow S_1$ transition with its dipole moment oriented along the long axis, and this remains the case when APTS converts into its S_1 conjugate photobase form. The femtosecond UV/IR pump-probe measurements (see Supporting Information) also show that there are no indications of electronic state configurations changes on

(sub)picosecond time scales, as the IR fingerprint patterns only show changes that occur with 84 ± 4 ps time constant in accordance with the photoacid APTS S_1 $R\text{-ND}_3^+ \rightarrow S_1$ $R\text{-ND}_2$ excited state deuteron transfer reaction, and initially optically excited state APTS S_1 $R\text{-ND}_3^+$ does not exhibit e.g. ${}^1L_a \leftrightarrow {}^1L_b$ population exchange kinetics, as has been shown for other photoacid chromophores.^[22]

Based on our experimental UV-XAS and UV-IR pump-probe findings, we can now refine our understanding of the electronic structure changes of APTS along the four stages of the Förster cycle. Our assessment of the electronic excited states of APTS using the CASSCF/NEVPT(6,7) level of theory shows that the S_1 state of the photoacid APTS has predominantly HOMO \rightarrow LUMO character and a minor contribution from HOMO \rightarrow LUMO + 2 (see electronic configurations given in Figure 4a), with the relative contributions of LUMO and LUMO + 2 CASSCF configurations changing when APTS converts into the conjugate photobase S_1 state (see also Supporting Information). Instead, the S_2 state is predominantly characterized by a HOMO \rightarrow LUMO + 1 excitation, with a minor contribution from a HOMO - 1 \rightarrow LUMO transition.

Calculations of the relevant states to describe the nitrogen K-edge XAS of photoacid $R\text{-NH}_3^+$ and conjugate photobase $R\text{-NH}_2$ forms of APTS reveal that for APTS in the S_0 state the lowest energy peak in the nitrogen K-edge spectrum with transitions to the core-excited X_1 state ($S_0 \rightarrow X_1$ transitions) is due to a one-electron nitrogen $1s \rightarrow$ LUMO excitation. In the S_1 state the dominant configuration involves a hole in the HOMO and an electron in the LUMO. Exciting an electron from the nitrogen $1s$ core orbital to fill up the hole in the HOMO in the S_1 state would therefore result in the same final X_1 state. This $S_1 \rightarrow X_1$ $1s$ core excitation requires less energy than $S_0 \rightarrow X_1$, because it is a $1s \rightarrow$ HOMO transition rather than $1s \rightarrow$ LUMO transition, making it frequency red-shifted by 3.3 eV or 2.9 eV for APTS in its photoacid or in its photobase forms, respectively, as our calculations predict. The photoacid $R\text{-NH}_3^+$ has a 20-fold smaller cross section for these transitions than the conjugate photobase $R\text{-NH}_2$ form of APTS. The next peak in the nitrogen K-edge XAS of APTS in the S_0 state is due to contributions by $S_0 \rightarrow X_3$ and X_4 states originating from one electron transitions from the nitrogen $1s$ core to LUMO + 2 and LUMO + 3, respectively. These X_3 and X_4 states are also accessible from the S_1 state by a similar one electron excitation schemes as discussed above, and also appear in the S_1 spectra with similar red-shifted transition frequencies. Electronic excitation to the S_2 state on the other hand would lead to the appearance of an X_2 signature indicative of a one electron excitation from nitrogen $1s$ to the HOMO.

We can now use the explanation for the pre-edge XAS peaks in the steady-state nitrogen K-edge spectra of S_0 APTS in its acid $R\text{-ND}_3^+$ and base $R\text{-ND}_2$ forms (see below) to also elucidate the electronic structure changes that drive photoacidity in the S_1 state and throughout the Förster cycle. In the photoacid $R\text{-NH}_3^+$ form in both the electronic S_0 and S_1 states, the missing lone pair on the nitrogen of the protonated amine group, and with it the missing hybrid-

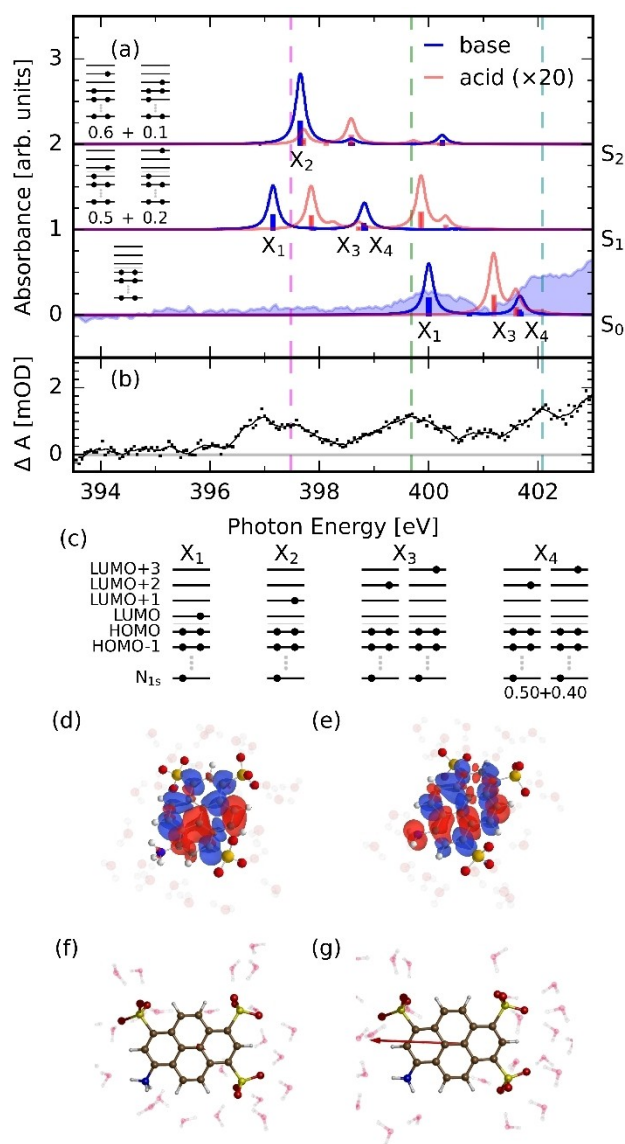


Figure 4. a) Comparison of the excited states involved the X-ray probing of APTS in its photoacid (red curves) and its conjugate photobase forms (blue curves) for the electronic S_0 ground and S_1 and S_2 electronic excited states. Please note the 20-fold increase in absorption strength of the $1s$ core \rightarrow LUMO excitations for APTS in its photobase form compared to those of APTS in its photoacid form. The theoretical spectra, calculated with NEVPT2, have been calibrated by a comparison of the lowest energy pre-edge transition of APTS photobase in the S_0 state as measured experimentally (blue shaded spectrum). b) With the same energy calibration a satisfying comparison results for the calculated and experimental spectra of APTS photobase in the S_1 state. c) Graphical representation of the most important involvement of the HOMOs and LUMOs of APTS for the particular $1s$ core excitations probed with (transient) N K-edge spectroscopy. Electronic charge distribution changes upon $S_0 \rightarrow S_1$ electronic excitation of APTS in its photoacid (d) and photobase (e) forms (Isovalue 0.0006 with red being positive). Electrical dipole moment changes from the CASSCF(6,7) level upon $S_0 \rightarrow S_1$ electronic excitation of APTS in its photoacid (f) and photobase (g) forms are 0.334 D and 4.701 D, respectively.

ization with the aromatic $\pi_{1,2}^*$ orbitals located predominantly on the pyrene backbone leads to an effective

electronic decoupling of the protonated amine group from the aromatic $\pi_{1,2...}^*$ pyrene orbitals. This decoupling results in minor cross section magnitudes for the nitrogen 1s pre-edge core excitations. It also means that upon electronic excitation the electronic structure around the protonated amine-group of APTS is not strongly altered, in agreement with our experimental observations. In contrast, when APTS $R-ND_3^+$ converts into its conjugate photobase $R-ND_2$ form, an about 20-fold increase of absorption cross sections for the core excited states X_1 , X_3 and X_4 occur, because of the availability of the amine nitrogen lone pair for conjugation with the $\pi_{1,2...}^*$ orbitals of the pyrene backbone. The X_1 state that can be reached from both S_0 and S_1 states, shifts in energy accordingly when being probed from either the S_0 or the S_1 states, and can be correlated to the energy difference between the S_0 and S_1 states. This difference in absorption cross section magnitude for the peak located at 397.4 eV of APTS in photoacid or photobase forms is therefore indicative of the appearance of the hole in the HOMO in the S_1 conjugate base $R-ND_2$ state as driven by the nitrogen lone pair hybridizing with the pyrene backbone. The rise of this peak accordingly follows the population kinetics of photoexcited APTS undergoing deuteron transfer to the solvent. A similar argument can be given for the temporal behaviour of the other peaks observed as transient absorption or bleaching signals.

We find that optical excitation of APTS $R-ND_3^+$ on the photoacid side only induces minor charge distribution changes at the amine group, whereas for APTS $R-ND_2$ in its conjugate photobase form these changes are substantial. With our calculations we conclude that these charge distribution changes are a direct consequence of the degree of conjugation of the amine group with the π bonding and π^* anti-bonding molecular orbitals predominantly located on the aromatic pyrene backbone is most profound when APTS is on the photobase side of the Förster cycle. This is exemplified in Figure 4d,e, where charge density changes upon optical excitation of APTS are depicted. Optical excitation leads to stronger electronic charge density changes in the amine group for APTS in its conjugate photobase $R-ND_2$ form than its photoacid $R-ND_3^+$ counterpart. This suggests a confirmation of the picture of photoacidity predominantly driven by electronic charge density changes occurring on the photobase side of the Förster cycle. However, the changes for particular carbon atoms in the pyrene backbone are much larger, as an estimate of the changes in Mulliken charges indicate (see Supporting Information). Indeed, according to our CASSCF calculations, the change in dipole moment upon electronic excitation is about 14 times larger for the photobase $R-ND_2$ form than for its photoacid $R-ND_3^+$ counterpart, resulting in clearly larger changes in solvation energies for the photobase $R-ND_2$. These results demonstrate the combined effects of local charge density changes of the proton donating/accepting functional groups and electrical dipole moments upon photoexcitation to be the key factors in the photoacidity phenomenon for the cationic photoacid APTS.

Conclusion

Summarizing, we have investigated the charge distribution changes upon optical excitation of the $S_0 \rightarrow S_1$ (HOMO \rightarrow LUMO) transition of an amine photoacid, APTS, with subsequent proton transfer along the four stages of the Förster cycle, by use of a local probe of nitrogen 1s core excitations to unoccupied molecular orbitals. Picosecond nitrogen K-edge absorption spectroscopy reveals the spectral signatures of the pre-edge bands (energy positions, cross sections) indicative of core-electron transitions to π^* orbitals. Our soft-X-ray local probe of the amine group provides direct access to the electronic structure and orbital interactions of proton donating/accepting groups. Our results pave the way for future electronic structure studies of acid-base reaction dynamics.

Acknowledgements

S. Eckert, M.-O. Winghart, C. Kleine, M. Ekimova, J. Ludwig and E.T.J. Nibbering acknowledge support from the German Science Foundation (Project Nr. DFG—NI 492/11-1) and the European Research Council (ERC) under the European Union's Horizon 2020 research and innovation programme (ERC Grant Agreement N° 788704; E.T.J.N.). A. Banerjee and M. Odelius acknowledges support from the Carl Tryggers Foundation (contract CTS18:285) and the European Union's Horizon 2020 research and innovation programme under the Marie Skłodowska-Curie grant agreement No 860553 and the Swedish Research Council (VR contract 2021-04521). DATA AVAILABILITY: The data sets generated and analyzed during the current study are available from the corresponding author on reasonable request. The calculations were enabled by resources provided by the Swedish National Infrastructure for Computing (SNIC) partially funded by the Swedish Research Council through grant agreement no. 2018-05973. J. Harich and N. Huse gratefully acknowledge funding from the Deutsche Forschungsgemeinschaft within the Sonderforschungsbereich 925 (project A4). E. Pines acknowledges support from the Israel Science Foundation (grant number 1587/16). We all greatly acknowledge the support of the BESSYII staff during x-ray measurements at the UE52_SGM Undulator SGM variable polarisation beamline of the Helmholtz-Zentrum Berlin and we thank Helmholtz-Zentrum Berlin for the allocation of synchrotron radiation beamtime. Open Access funding enabled and organized by Projekt DEAL.

Conflict of Interest

The authors declare no conflict of interest.

Data Availability Statement

The data that support the findings of this study are available from the corresponding author upon reasonable request.

Keywords: Aromaticity · Electronic Structure · Orbital Interactions · Photoacids · Time-Resolved Soft x-Ray Spectroscopy

- [1] a) E. Pines, D. Huppert, N. Agmon, *J. Chem. Phys.* **1988**, *88*, 5620–5630; b) N. Agmon, E. Pines, D. Huppert, *J. Chem. Phys.* **1988**, *88*, 5631–5638; c) L. Genosar, B. Cohen, D. Huppert, *J. Phys. Chem. A* **2000**, *104*, 6689–6698; d) M. Rini, B.-Z. Magnes, E. Pines, E. T. J. Nibbering, *Science* **2003**, *301*, 349–352; e) O. F. Mohammed, D. Pines, J. Dreyer, E. Pines, E. T. J. Nibbering, *Science* **2005**, *310*, 83–86; f) O. F. Mohammed, D. Pines, E. T. J. Nibbering, E. Pines, *Angew. Chem. Int. Ed.* **2007**, *46*, 1458–1461; *Angew. Chem.* **2007**, *119*, 1480–1483; g) K. Adamczyk, M. Prémont-Schwarz, D. Pines, E. Pines, E. T. J. Nibbering, *Science* **2009**, *326*, 1690–1694; h) B. J. Siwick, M. J. Cox, H. J. Bakker, *J. Phys. Chem. B* **2008**, *112*, 378–389; i) E. Pines, D. Pines, Y.-Z. Ma, G. R. Fleming, *ChemPhysChem* **2004**, *5*, 1315–1327; j) D. B. Spry, M. D. Fayer, *J. Chem. Phys.* **2008**, *128*, 084508; k) L. N. Silverman, D. B. Spry, S. G. Boxer, M. D. Fayer, *J. Phys. Chem. A* **2008**, *112*, 10244–10249.
- [2] a) E. Pines, G. R. Fleming, *J. Phys. Chem.* **1991**, *95*, 10448–10457; b) C. Spies, S. Shomer, B. Finkler, D. Pines, E. Pines, G. Jung, D. Huppert, *Phys. Chem. Chem. Phys.* **2014**, *16*, 9104–9114; c) M. Ekimova, F. Hoffmann, G. Bekçioğlu-Neff, A. Rafferty, O. Kornilov, E. T. J. Nibbering, D. Sebastiani, *J. Am. Chem. Soc.* **2019**, *141*, 14581–14592; d) M.-A. Codescu, M. Weiss, M. Brehm, O. Kornilov, D. Sebastiani, E. T. J. Nibbering, *J. Phys. Chem. A* **2021**, *125*, 1845–1859; e) T. Kumpulainen, A. Rosspeintner, B. Dereka, E. Vauthey, *J. Phys. Chem. Lett.* **2017**, *8*, 4516–4521; f) P. Verma, A. Rosspeintner, B. Dereka, E. Vauthey, T. Kumpulainen, *Chem. Sci.* **2020**, *11*, 7963–7971.
- [3] a) D. B. Spry, A. Goun, K. Glusac, D. E. Moilanen, M. D. Fayer, *J. Am. Chem. Soc.* **2007**, *129*, 8122–8130; b) D. B. Spry, M. D. Fayer, *J. Phys. Chem. B* **2009**, *113*, 10210–10221.
- [4] a) D. Stoner-Ma, A. A. Jaye, P. Matousek, M. Towrie, S. R. Meech, P. J. Tonge, *J. Am. Chem. Soc.* **2005**, *127*, 2864–2865; b) B. Salna, A. Benabbas, J. T. Sage, J. van Thor, P. M. Champion, *Nat. Chem.* **2016**, *8*, 874–880.
- [5] a) T. Förster, *Naturwissenschaften* **1949**, *36*, 186–187; b) T. Förster, *Z. Elektrochem.* **1950**, *54*, 531–535; c) Z. R. Grabowski, A. Grabowska, *Z. Phys. Chem.* **1976**, *101*, 197–208.
- [6] S. G. Schulman, *Spectrosc. Lett.* **1973**, *6*, 197–202.
- [7] a) G. Granucci, J. T. Hynes, P. Millié, T.-H. Tran-Thi, *J. Am. Chem. Soc.* **2000**, *122*, 12243–12253; b) J. T. Hynes, T. H. Tran-Thi, G. Granucci, *J. Photochem. Photobiol. A* **2002**, *154*, 3–11; c) N. Agmon, W. Rettig, C. Groth, *J. Am. Chem. Soc.* **2002**, *124*, 1089–1096.
- [8] M. Rosenberg, C. Dahlstrand, K. Kilså, H. Ottosson, *Chem. Rev.* **2014**, *114*, 5379–5425.
- [9] Z. Wen, L. J. Karas, C.-H. Wu, J. I.-C. Wu, *Chem. Commun.* **2020**, *56*, 8380–8383.
- [10] B. T. Psciuk, M. Prémont-Schwarz, B. Koeppe, S. Keinan, D. Xiao, E. T. J. Nibbering, V. S. Batista, *J. Phys. Chem. A* **2015**, *119*, 4800–4812.
- [11] a) S. Eckert, J. Norell, P. S. Miedema, M. Beye, M. Fondell, W. Quevedo, B. Kennedy, M. Hantschmann, A. Pietzsch, B. E. Van Kuiken, M. Ross, M. P. Minitti, S. P. Moeller, W. F. Schlotter, M. Khalil, M. Odelius, A. Föhlisch, *Angew. Chem. Int. Ed.* **2017**, *56*, 6088–6092; *Angew. Chem.* **2017**, *129*, 6184–6188; b) S. Eckert, J. Norell, R. M. Jay, M. Fondell, R. Mitzner, M. Odelius, A. Föhlisch, *Chem. Eur. J.* **2019**, *25*, 1733–1739.
- [12] D. Pines, E. Pines in *Hydrogen-Transfer Reactions, Vol. I: Physical and Chemical Aspects I–III* (Eds.: J. T. Hynes, J. P. Klinman, H.-H. Limbach, R. L. Schowen), Wiley-VCH, Weinheim, **2007**, pp. 377–415.
- [13] “ ברק צביה תמר מאת/בתמיסת נייטרליות וחומצות קטיוניות בחומצות פרוטון ” (Dynamics and Thermodynamics Aspects of Proton Transfer from Cationic and Neutral Photoacids in Solutions): T. Z. Barak, Ben Gurion University of the Negev (Beersheva, Israel), **2005**.
- [14] M. Ekimova, W. Quevedo, M. Faubel, P. Wernet, E. T. J. Nibbering, *Struct. Dyn.* **2015**, *2*, 054301.
- [15] a) P. S. Miedema, W. Quevedo, M. Fondell, *Journal of Large-Scale Research Facilities* **2016**, *2*, A70; b) M. Fondell, S. Eckert, R. M. Jay, C. Weniger, W. Quevedo, J. Niskanen, B. Kennedy, F. Sorgenfrei, D. Schick, E. Giangrisostomi, R. Ovsyannikov, K. Adamczyk, N. Huse, P. Wernet, R. Mitzner, A. Föhlisch, *Struct. Dyn.* **2017**, *4*, 054902.
- [16] T. Yanai, D. P. Tew, N. C. Handy, *Chem. Phys. Lett.* **2004**, *393*, 51–57.
- [17] C. Angeli, R. Cimraglia, S. Evangelisti, T. Leininger, J. P. Malrieu, *J. Chem. Phys.* **2001**, *114*, 10252–10264.
- [18] F. Neese, F. Wennmohs, U. Becker, C. Riplinger, *J. Chem. Phys.* **2020**, *152*, 224108.
- [19] a) M. Ekimova, W. Quevedo, Ł. Szyc, M. Iannuzzi, P. Wernet, M. Odelius, E. T. J. Nibbering, *J. Am. Chem. Soc.* **2017**, *139*, 12773–12783; b) M. Ekimova, M. Kubin, M. Ochmann, J. Ludwig, N. Huse, P. Wernet, M. Odelius, E. T. J. Nibbering, *J. Phys. Chem. B* **2018**, *122*, 7737–7746.
- [20] J. R. Platt, *J. Chem. Phys.* **1949**, *17*, 484–495.
- [21] M. K. Roos, S. Reiter, R. de Vivie-Riedle, *Chem. Phys.* **2018**, *515*, 586–595.
- [22] F. Messina, M. Prémont-Schwarz, O. Braem, D. Q. Xiao, V. S. Batista, E. T. J. Nibbering, M. Chergui, *Angew. Chem. Int. Ed.* **2013**, *52*, 6871–6875; *Angew. Chem.* **2013**, *125*, 7009–7013.

Manuscript received: January 14, 2022

Accepted manuscript online: March 24, 2022

Version of record online: April 27, 2022